A Generalized Rusanov method for Saint-Venant Equations with Variable Horizontal Density

Fayssal Benkhaldoun, Kamel Mohamed, and Mohammed Seaïd

Abstract We present a class of finite volume methods for the numerical solution of Saint-Venant equations with variable horizontal density. The model is based on coupling the Saint-Venant equations for the hydraulic variables with a suspended sediment transport equation for the concentration variable. To approximate the numerical solution of the considered models we propose a generalized Rusanov method. The method is simple, accurate and avoids the solution of Riemann problems during the time integration process. Using flux limiters, a second-order accuracy is achieved in the reconstruction of numerical fluxes. The proposed finite volume method is well-balanced, conservative, non-oscillatory and suitable for Saint-Venant equations for which Riemann problems are difficult to solve. The numerical results are presented for two test examples.

Keywords Shallow water equations, variable density, finite volume method
MSC2010: 35L04, 65N08, 76L05

1 Introduction

In this paper we are interested to develop a robust finite volume method for solving Saint-Venant equations with variable horizontal density. The governing equations

Fayssal Benkhaldoun
LAGA, Université Paris 13, 99 Av J.B. Clement, 93430 Villetaneuse, France,
e-mail: fayssal@math.univ-paris13.fr

Kamel Mohamed
Department of Computer Science, Faculty of Applied Sciences, University of Taibah, Madinah KSA, e-mail: kamel16@yahoo.com

Mohammed Seaïd
School of Engineering and Computing Sciences, University of Durham, South Road, Durham DH1 3LE, UK, e-mail: m.seaid@durham.ac.uk

J. Fořt et al. (eds.), *Finite Volumes for Complex Applications VI – Problems & Perspectives*, Springer Proceedings in Mathematics 4,
DOI 10.1007/978-3-642-20671-9_10,

can be formulated in a conservative form as

$$\frac{\partial \mathbf{W}}{\partial t} + \frac{\partial \mathbf{F}(\mathbf{W})}{\partial x} = \mathbf{Q}(\mathbf{W}), \tag{1}$$

where $\mathbf{W}$, $\mathbf{F}(\mathbf{W})$ and $\mathbf{Q}(\mathbf{W})$ are vector-valued functions in $\mathbb{R}^3$ given by

$$\mathbf{W} = \begin{pmatrix} \rho h \\ \rho h u \\ \rho_s h c \end{pmatrix}, \qquad \mathbf{F}(\mathbf{W}) = \begin{pmatrix} \rho h u \\ \rho h u^2 + \frac{1}{2} g \rho h^2 \\ \rho_s h u c \end{pmatrix}, \qquad \mathbf{Q}(\mathbf{W}) = \begin{pmatrix} 0 \\ -g \rho h \frac{\partial Z}{\partial x} \\ 0 \end{pmatrix},$$

where h is the water height above the bottom, u the water velocity, g the acceleration due to gravity, Z the function characterizing the bottom topography and ρ_s the sediment density. For constant density ρ, the equations (1) reduce to the standard Saint-Venant equations. In the current work, we assume that a sediment transport takes place such that the density depends on space and time variables, *i.e.*, $\rho = \rho(x, t)$. This requires an additional equation for its evolution. Here, the equation used to close the system is given by

$$\rho = \rho_w + (\rho_s - \rho_w)\, c, \tag{2}$$

where ρ_s is the sediment density and c is the depth-averaged concentration of the suspended sediment. Further details on the formulation of the above equations we refer to [3] and further references are therein. It is clear that the system (1) is hyperbolic and the associated eigenvalues λ_k ($k = 1, 2, 3$) are

$$\lambda_1 = u - \sqrt{gh}, \qquad \lambda_2 = u \qquad \text{and} \qquad \lambda_3 = u + \sqrt{gh}. \tag{3}$$

Note that in the above hydrodynamical model, we have considered only the source terms related to bottom topography while the source terms related to bed friction are neglected. Moreover, the bed-load sediment transport is assumed to be negligible in the considered model compared to the suspended sediment load. It should also be stressed that the transport of suspended sediments involves different physical mechanisms occurring within different time scales according to their time response to the hydrodynamics. In practice, the sediment transport of the bed occurs on a transport time scale much longer than the flow time scale. It is therefore desirable to construct numerical schemes that preserve stability for all time scales. In the current study we propose a modified Rusanov method studied and analyzed in [1] for the numerical solution of conservation laws with source terms. This method is simple, accurate and avoids the solution of Riemann problems during the time integration process. Our main goal is to present a class of numerical methods that are simple, easy to implement, and accurately solves the Saint-Venant equations with variable horizontal density without relying on Riemann solvers or front tracking techniques.

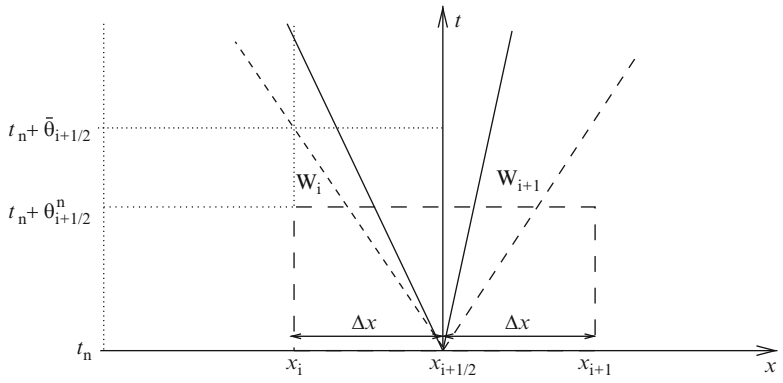

Fig. 1 An illustration of modified Riemann problems in the proposed finite volume method

2 A generalized Rusanov method

To formulate our finite volume method, we discretize the spatial domain into control volumes $[x_{i-1/2}, x_{i+1/2}]$ with uniform size $\Delta x = x_{i+1/2} - x_{i-1/2}$ and we divide the temporal domain into subintervals $[t_n, t_{n+1}]$ with uniform size Δt. Following the standard finite volume formulation, we integrate the equation (1) with respect to time and space over the domain $[t_n, t_{n+1}] \times [x_{i-1/2}, x_{i+1/2}]$ to obtain the following discrete equation

$$\mathbf{W}_i^{n+1} = \mathbf{W}_i^n - \frac{\Delta t}{\Delta x}\left(\mathbf{F}(\mathbf{W}_{i+1/2}^n) - \mathbf{F}(\mathbf{W}_{i-1/2}^n)\right) + \Delta t \mathbf{Q}_i^n, \tag{4}$$

where $\mathbf{W}_i^n$ is the time-space average of the solution $\mathbf{W}$ in the domain $[x_{i-1/2}, x_{i+1/2}]$ at time t_n and $\mathbf{F}(\mathbf{W}_{i\pm1/2}^n)$ is the numerical flux at $x = x_{i\pm1/2}$ and time t_n. The spatial discretization of the equation (4) is complete when a numerical construction of the fluxes $\mathbf{F}(\mathbf{W}_{i\pm1/2}^n)$ is chosen and a discretization of the source term $\mathbf{Q}_i^n$ is performed. In general, the construction of numerical fluxes requires a solution of Riemann problems at the interfaces $x_{i\pm1/2}$.

In order to avoid these difficulties and reconstruct an approximation of $\mathbf{W}_{i+1/2}^n$, we adapt a finite volume method proposed in [1] for numerical solution of conservation laws with source terms. The key idea is to integrate the equation (1) over a control domain $[t_n, t_n + \theta_{i+1/2}^n] \times [x_i, x_{i+1}]$ containing the point $(t_n, x_{i+1/2})$ as depicted in Fig. 1. It should be stressed that, the integration of the equation (1) over the control domain $[t_n, t_n + \theta_{i+1/2}^n] \times [x_i, x_{i+1}]$ is used only at a predictor stage to construct the intermediate states $\mathbf{W}_{i\pm1/2}^n$ which will be used in the corrector stage (4). Here, $\mathbf{W}_{i\pm1/2}^n$ can be viewed as an approximation of the averaged Riemann solution over the control volume $[x_i, x_{i+1}]$ at time $t_n + \theta_{i+1/2}^n$. Thus, the resulting intermediate state is given by

$$\mathbf{W}_{i+1/2}^{n} = \frac{1}{2}\left(\mathbf{W}_{i}^{n} + \mathbf{W}_{i+1}^{n}\right) - \frac{\theta_{i+1/2}^{n}}{\Delta x}\Big(F(\mathbf{W}_{i+1}^{n}) - F(\mathbf{W}_{i}^{n})\Big) + \theta_{i+1/2}^{n} Q_{i+1/2}^{n}, \quad (5)$$

where $Q_{i+1/2}^{n}$ is an approximation of the averaged source term Q *i.e.*

$$Q_{i+1/2}^{n} = \frac{1}{\theta_{i+1/2}^{n}\Delta x}\int_{t_n}^{t_n+\theta_{i+1/2}^{n}}\int_{x_i}^{x_{i+1}} Q(\mathbf{W})\, dt\, dx.$$

In order to complete the implementation of the above finite volume method the parameters $\theta_{i+1/2}^{n}$ and $Q_{i+1/2}^{n}$ have to be selected. Based on the stability analysis reported in [1] for conservation laws with source terms, the variable $\theta_{i+1/2}^{n}$ is selected as

$$\theta_{i+1/2}^{n} = \alpha_{i+1/2}^{n}\bar{\theta}_{i+1/2}, \qquad \bar{\theta}_{i+1/2} = \frac{\Delta x}{2S_{i+1/2}^{n}}, \quad (6)$$

where $\alpha_{i+1/2}^{n}$ is a positive parameter to be calculated locally and $S_{i+1/2}^{n}$ is the local Rusanov's velocity defined as

$$S_{i+1/2}^{n} = \max_{k=1,2,3}\left(\max\left(\left|\lambda_{k,i}^{n}\right|, \left|\lambda_{k,i+1}^{n}\right|\right)\right), \quad (7)$$

with $\lambda_{k,i}^{n}$ is the kth eigenvalue in (3) evaluated at the solution state $\mathbf{W}_{i}^{n}$. Notice that the introduction of the local time step $\theta_{i+1/2}^{n}$ in the predictor stage (5) is motivated by the fact that $\theta_{i+1/2}^{n}$ should not be larger than the value $\bar{\theta}_{i+1/2}$ which corresponds to the time required for the fastest wave generated at the interface $x_{i+1/2}$ to leave the cell $[x_i, x_{i+1}]$, compare Fig. 1.

It is clear that by setting $\alpha_{i+1/2}^{n} = 1$ the proposed finite volume method reduces to the well-established Rusanov method for linear systems of conservation laws, whereas for $\alpha_{i+1/2}^{n} = \Delta t/\Delta x S_{i+1/2}^{n}$ one recovers the well-known Lax-Wendroff scheme. Another choice of the slopes $\alpha_{i+1/2}^{n}$ leading to a first-order scheme is $\alpha_{i+1/2}^{n} = \tilde{\alpha}_{i+1/2}^{n}$ with

$$\tilde{\alpha}_{i+1/2}^{n} = \frac{S_{i+1/2}^{n}}{s_{i+1/2}^{n}}, \quad (8)$$

where

$$s_{i+1/2}^{n} = \min_{k=1,2,3}\left(\min\left(\left|\lambda_{k,i}^{n}\right|, \left|\lambda_{k,i+1}^{n}\right|\right)\right). \quad (9)$$

In the current study we incorporate limiters in its reconstruction as

$$\alpha_{i+1/2}^{n} = \tilde{\alpha}_{i+1/2}^{n} + \sigma_{i+1/2}^{n}\Phi\left(r_{i+1/2}\right), \quad (10)$$

where $\tilde{\alpha}_{i+1/2}^{n}$ is given by (8) and $\Phi_{i+1/2} = \Phi\left(r_{i+1/2}\right)$ is an appropriate limiter which is defined by using a flux limiter function Φ acting on a quantity that measures the ratio $r_{i+1/2}$ of the upwind change to the local change, see for instance [6]. In the

present study,

$$\sigma^n_{i+1/2} = \frac{\Delta t}{\Delta x} S^n_{i+1/2} - \frac{S^n_{i+1/2}}{s^n_{i+1/2}},$$

and the ratio of the upwind change is calculated locally as

$$r_{i+1/2} = \frac{W_{i+1-q} - W_{i-q}}{W_{i+1} - W_i}, \qquad q = \text{sgn}\left[\tilde{\alpha}^n_{i+1/2}\right].$$

As a slope limiter function, we consider the Minmod function

$$\Phi(r) = \max\left(0, \min\left(1, r\right)\right). \tag{11}$$

Note that other slope limiter functions functions from [4, 6] can also apply. The reconstructed slopes (10) are inserted in (6) and the numerical fluxes $\mathbf{W}^n_{i+1/2}$ are computed from (5). Remark that if we set $\Phi = 0$, the spatial discretization (10) reduces to the first-order scheme.

3 Numerical Results

Two test examples are selected to check the accuracy and the performance of the proposed finite volume scheme. As with all explicit time stepping methods the theoretical maximum stable time step Δt is specified according to the Courant-Friedrichs-Lewy condition

$$\Delta t = Cr \frac{\Delta x}{\max\limits_i \left(\left|\alpha^n_{i+1/2}\right|\right)}, \tag{12}$$

where Cr is a constant to be chosen less than unity. In all our simulations, the fixed Courant number $Cr = 0.5$ is used and the time step is varied according to (12).

3.1 Example 1

We consider a density dam-break problem with a single initial discontinuity. The problem consists of solving the equations (1) in a flat channel of length 500 m filled with two liquids with density $\rho = 10\ kg/m^3$ in the left section and $\rho = 1\ kg/m^3$ in the right section. Initially, the system is at rest with constant water height $h = 1\ m$ and $g = 1\ m/s^2$. In Fig. 2 we display the time evolution of the density, water height, velocity and concentration variables using a mesh with 500 gridpoints. It is clear from these results that at the initial time, the hydrostatic pressure difference at the interface of the two liquids drives a flow of higher density liquid towards the right,

pushing the lower density liquid ahead. To conserve mass, the free surface of the lower density liquid rises and a rightward propagating shock-like bore forms. This flow features have been accurately captured by our generalized Rusanov scheme. It should be stressed that the mechanisms of the density dam-break problems are similar to that of the standard dam-break induced by change in free-surface depth, in that a leftward rarefaction, a rightward shock and a contact wave are formed. Similar wave structures also occur in shock tube gas dynamics.

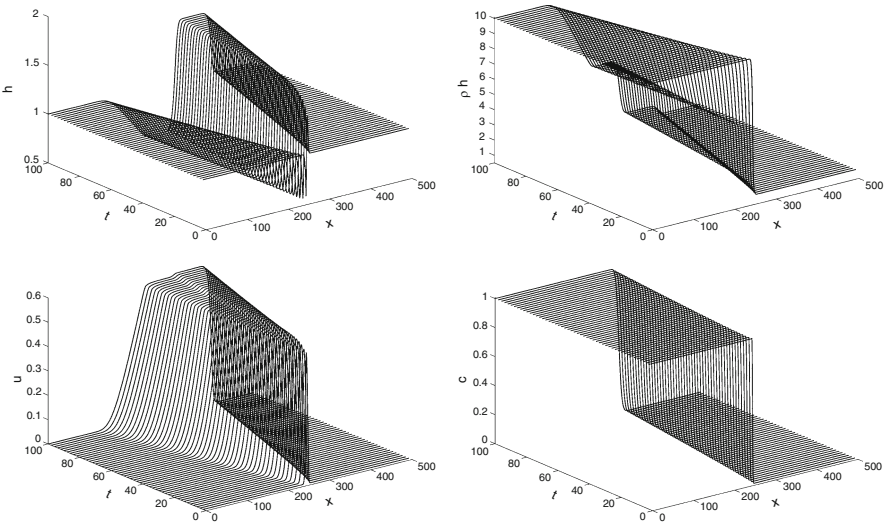

Fig. 2 Numerical results for density dam-break problem with a single initial discontinuity

For the sake of comparison, we present in Fig. 3 the results for the water height at $t = 70\ s$ obtained using the classical Rusanov method and the proposed method using a mesh with 500 and 1000 gridpoints. We have also included a reference solution obtained using a refined mesh with 100000 gridpoints. As can be seen from this figure, the results obtained using the classical Rusanov method are more diffusive than those obtained using our finite volume method. Similar conclusion can be drawn from other results (not reported here) obtained for the velocity field and sediment concentration.

3.2 Example 2

In this example we solve a density dam-break problem with two initial discontinuities. Here, a flat channel of length 100 m is filled at the left-hand side and right-hand side of the channel with a liquid with density $\rho = 1\ kg/m^3$. At the centre of the channel there is a liquid column of density $\rho = 10\ kg/m^3$ and width

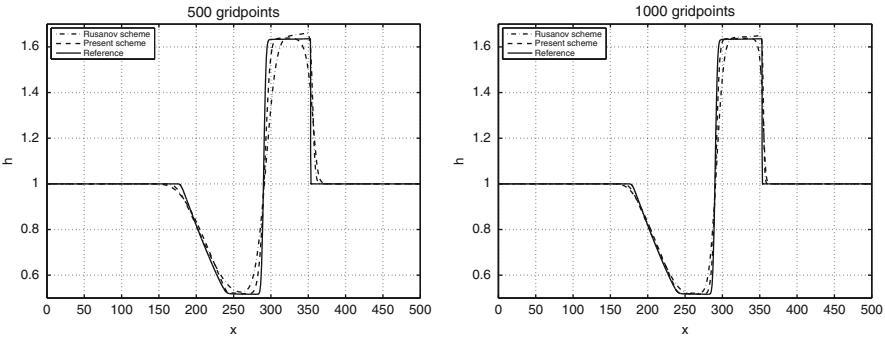

Fig. 3 Comparative results for the water height at $t = 70\ s$ for density dam-break problem with a single initial discontinuity using a mesh with 500 gridpoints (left) and 1000 gridpoints (right)

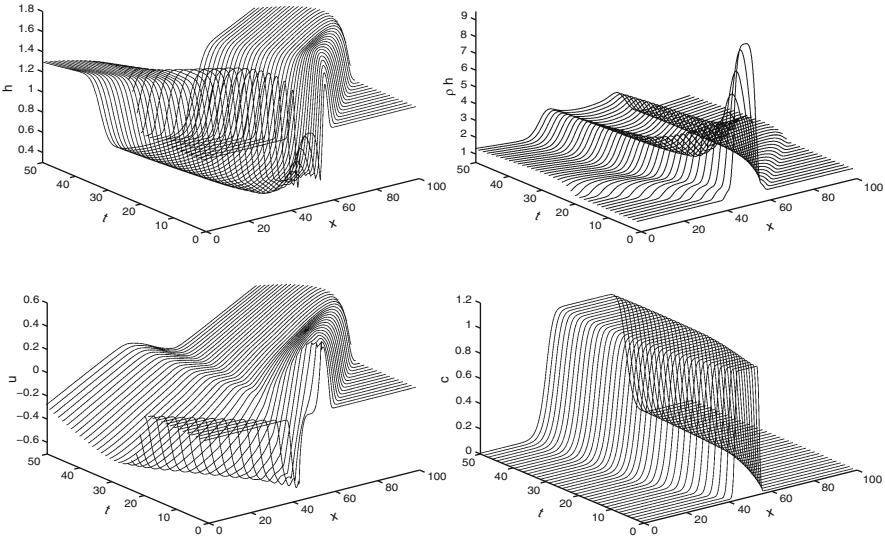

Fig. 4 Numerical results for density dam-break problem with two initial discontinuities

of 1 m. Initially, the system is at rest with constant water height $h = 1\ m$ and $g = 1\ m/s^2$. The computed results are illustrated in Fig. 4 for the t-x phase space. It is evident that the sudden collapse of the denser liquid in the central column causes primary shock waves to be created and propagate as bores in the direction from high to low density. Two outward propagating bores are generated, traveling in opposite directions. Each primary bore decreases in strength with time, which can be seen from the curved shock path. On the other hand, a pair of rarefaction waves travels inward from the interfaces. The rarefaction waves are almost immediately reflected at the center, and then move outward, weakening rapidly. The accuracy of the proposed finite volume is highly achieved in reproducing these physical features.

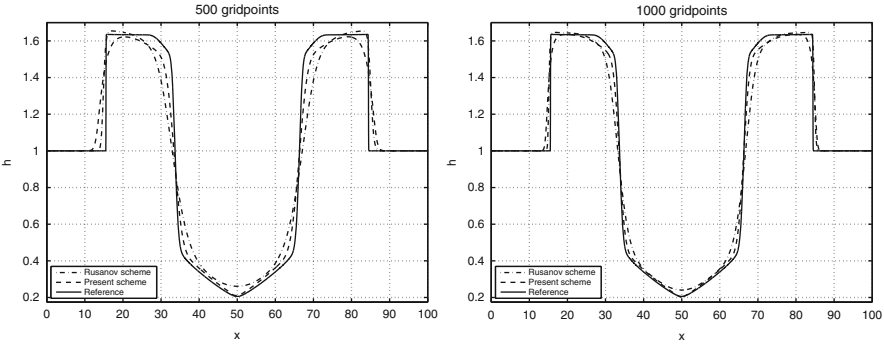

Fig. 5 Comparative results for the water height at $t = 20\ s$ for density dam-break problem with two initial discontinuities using a mesh with 500 gridpoints (left) and 1000 gridpoints (right)

In Fig. 5 we illustrate a comparison between the results for the water height at $t = 20\ s$ obtained using the classical Rusanov method and the proposed method using a mesh with 500 and 1000 gridpoints. Again, a reference solution obtained using a refined mesh with 100000 gridpoints is included in this figure. As in the previous test example, an excessive numerical diffusion is detected in the results obtained using the classical Rusanov method. This numerical diffusion has been noticeably reduced in the results obtained using the proposed finite volume method.

References

1. Mohamed, K.: Simulation numérique en volume finis, de problémes d'écoulements multidimensionnels raides, par un schéma de flux á deux pas. Dissertation, University of Paris 13, (2005)
2. Rusanov, V.: Calculation of interaction of non-steady shock waves with obstacles. Comp. Math. Phys. USSR. **1**, 267–279 (1961)
3. Leighton, F.Z. Borthwick, A.G.L. Taylor, P.H.: 1-D numerical modelling of shallow flows with variable horizontal density. International Journal for Numerical Methods in Fluids. **62**, 1209–1231 (2010)
4. Randall, J.L.: Numerical Methods for Conservation Laws, Lectures in Mathematics. ETH Zürich, (1992)
5. Roe, P.: Approximate riemann solvers, parameter vectors and difference schemes. J. Comp. Physics. **43**, 357–372 (1981)
6. Sweby, P.K.: High resolution schemes using flux limiters for hyperbolic conservation laws. SIAM J. Numer. Anal. **21**, 995–1011 (1984)

The paper is in final form and no similar paper has been or is being submitted elsewhere.